Supporting Information

Flexible, Bio-Compatible Nanofluidic Ion Conductor

Chengwei Wang,[1,a] Sha Wang,[1,a] Guang Chen,[2] Weiqing Kong,[1] Weiwei Ping,[1] Jiaqi Dai,[1] Glenn Pastel,[1] Hua Xie,[1] Shuaiming He,[1] Siddhartha Das,[2] Liangbing Hu[1,*]

[1]Department of Materials Science and Engineering, University of Maryland College Park, College Park, Maryland, 20742

[2]Department of Mechanical Engineering, University of Maryland College Park, College Park, Maryland, 20742

Email: binghu@umd.edu

[a] These authors contributed equally to this work.

Experiments

TEMPO-Mediated Oxidation of Cellulose. A piece of BC pellicle was put into solution (300 mL) containing TEMPO (0.02g/g) and sodium bromide (0.15g/g). A designed amount of the 12.5% NaClO solution, corresponding to 10 mmol/g cellulose (5mL/g), was added slowly to the cellulose slurry. And the pH was maintained at 10 at room temperature by adding 0.5 mol/L NaOH solution using a pH stat. The reaction was finished after no additional consumption of the alkali takes place. Then the oxidation was quenched by adding ethanol (ca. 5 mL). The oxidized BC was rinsed thoroughly with large amounts of water on a filter membrane set in a Büchner funnel until neutral pH.

Device Preparation. The press-dried BC and TEMPO-treated BC film were cut into a rectangular shape (~10 mm × 5 mm). Then a 5 mm wide glass slide was used to press the film on to a glass substrate using epoxy or PDMS as the glue. The thickness of the device is the thickness of the dry film (measured from the SEM image). The two ends of the film were exposed to ensure good contact with the electrodes. The as-made nanofluidic devices were soaked in different concentrations of NaCl solution for conductivity measurements. At each concentration, the devices were soaked more than 24 h to reach equilibrium. The conductivity measurements were conducted with a BioLogic VMP3 potentiostat. Two titanium strips were attached to the two ends of the nanofluidic device as the electrodes. The EIS was performed with a 50 mV AC amplitude in the frequency range of 500 mHz to 1 MHz. To fabricate a humidity sensor, a thin layer of CNTs was coated using 3 mg/mL CNTs in DMF solution on both sides of the TEMPO-treated BC film to act as the electrodes, and two conductive copper tapes were attached to the CNTs layer for electrical connection points. Then one side of the device was carefully immersed into the PDMS precursor to partially seal the device, while the other side was

left exposed to air. The PDMS was fully cured at about 100 ^{o}C. The humidity response measurement was conducted in an environmental chamber at different relative humidity. Nasal breathing tests were conducted about 20 cm above the sensor.

***Materials characterization*.** The morphologies of the BC film were conducted on a Tescan XEIA Plasma FIB/SEM at 10 kV. The nitrogen adsorption isotherm was measured using a Quantachrome Autosorb-1 instrument at a temperature of 77K, and the pore size distribution was calculated using density function theory (DFT). The zeta potentials of the BC before and after TEMPO treatment were measured with a Malvern Zetasizer (ZEN3690) instrument. BC and the TEMPO-oxidized BC dispersed in water first with a blender, then a probe sonicator for the zeta potential measurements. The capacitance of the humidity sensor was measured on a GLK instruments, Model 3000 Capacitance Meter.

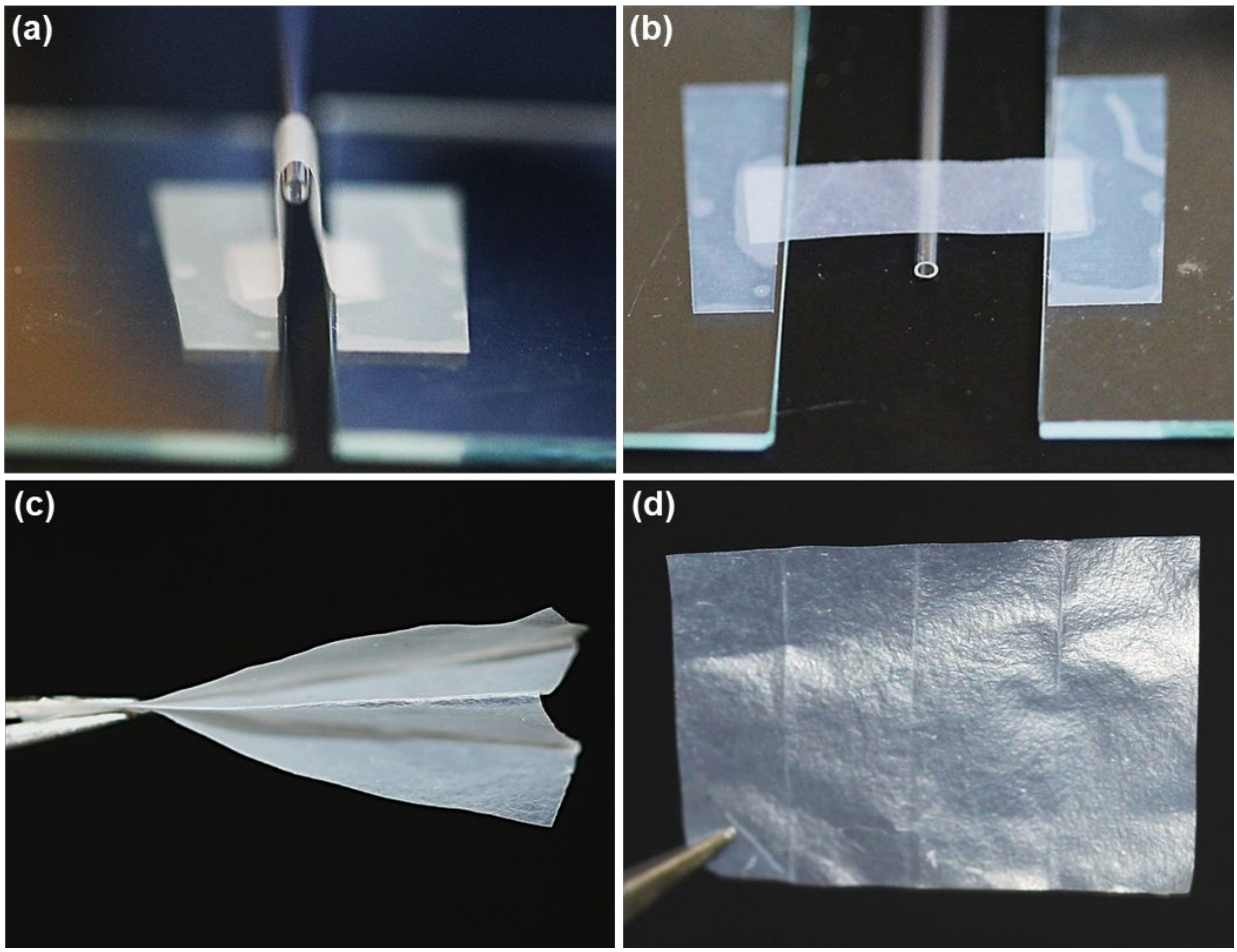

Figure S1. Photographs of the TEMPO-treated BC film (a) during and (b) after a bending test on a glass tube with a diameter of (1 mm). Photographs of (c) the folded TEMPO-treated BC film and (d) the film after unfolding.

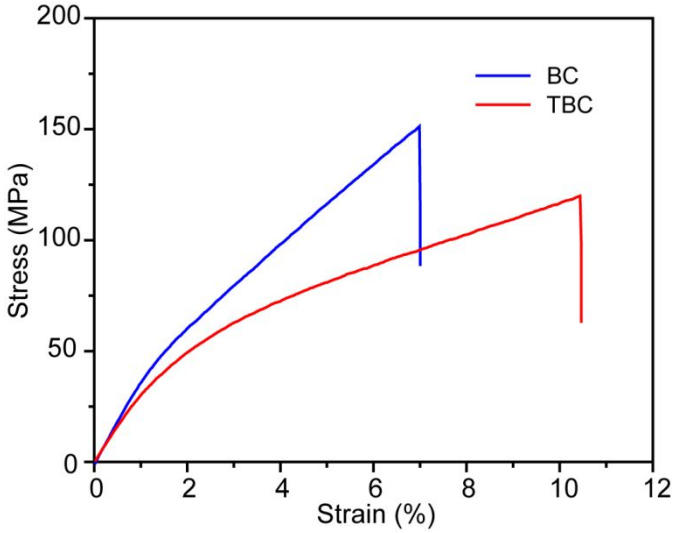

Figure S2. Strain-stress measurement of BC and TEMPO-treated BC films.

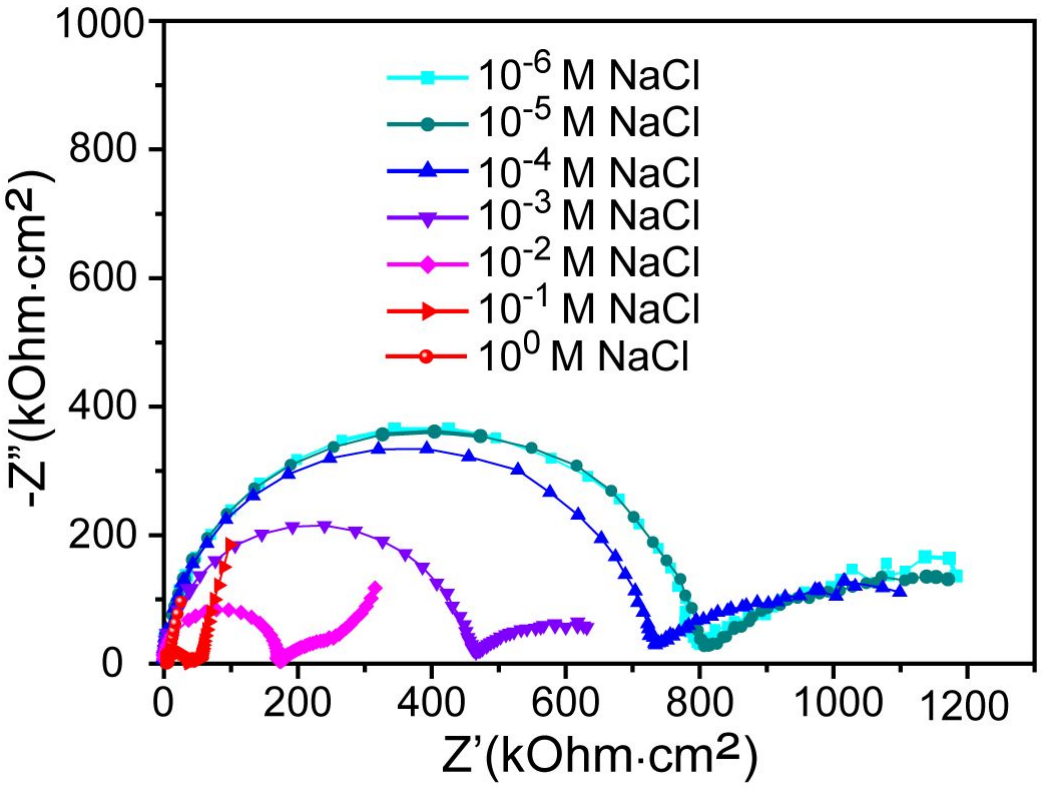

Figure. S3. Nyquist plot of the TEMPO-treated BC based nanofluidic device at different concentrations of the NaCl soaking solution. The decrease of radii of the semicircles indicates the increase in ionic conductivity.

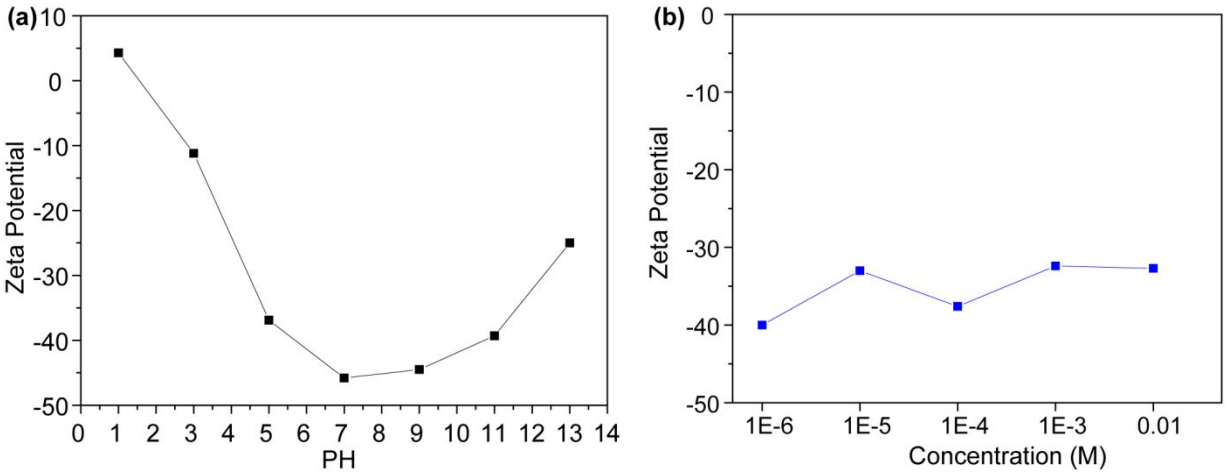

Figure S4. Zeta potentials of the TEMPO-oxidized BC as a function of (a) pH and (b) NaCl concentration.

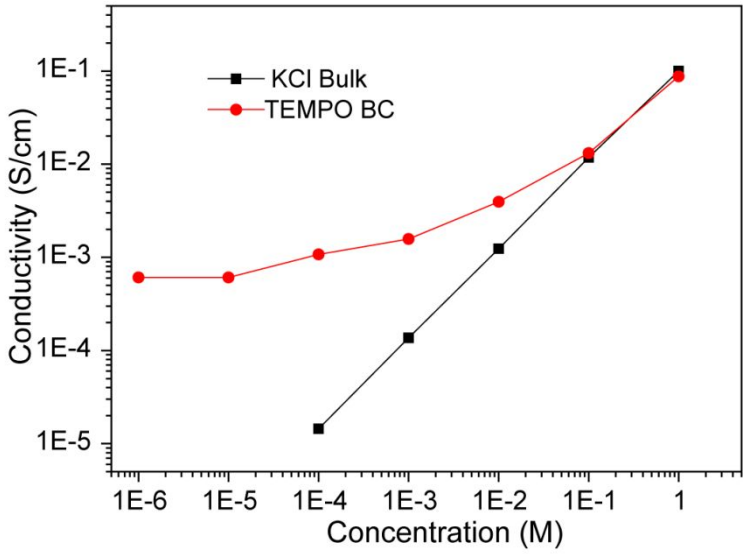

Figure S5. Ionic conductivity of the TEMPO-oxidized BC film in KCl.

Theory for the quantification of ionic conductivity in pristine BC and TEMPO BC

The nanofluidic spaces between the nanofibers of the BC are considered charged nanochannels of height 2h immersed in NaCl solution. Charging of the nanochannels is primarily atrtibuted to the pH-dependent ionization of–COOH groups[1,2]. Below, we first provide a derivation demonstrating how the buildup of charge leads to an interrelationship between the zeta potential and the surface charge density, as dictated by the pH and the ion concentration of the system. –COOH groups ionize as follows[1]:

$$R-COOH \leftrightarrow R-COO^- + H^+ \quad \left(\text{Equilibrium constant } K_a\right) \tag{S1}$$

$$R-COO^- + Na^+ \leftrightarrow R-COO^-Na^+ \quad \left(\text{Equilibrium constant } K_p\right) \tag{S2}$$

Using eqs.(S1,S2), we can related the concentrations c_i of all the species to the different equilibrium constants as:

$$K_a = \frac{\left(c_{R-COO^-}\right)\left(c_{H^+}\right)}{c_{R-COOH}} \Rightarrow c_{R-COOH} = \frac{\left(c_{R-COO^-}\right)\left(c_{H^+}\right)}{K_a}, \tag{S3}$$

$$K_p = \frac{c_{R-COO^-Na^+}}{\left(c_{R-COO^-}\right)\left(c_{Na^+}\right)} \Rightarrow c_{R-COO^-Na^+} = K_p\left(c_{R-COO^-}\right)\left(c_{Na^+}\right), \tag{S4}$$

It is critical to note here that the unit of K_a is mol/m^3 (1 M=1000 mol/m^3) and K_p is m^3/mol. Also, the species that exist only on the surface (e.g., $R-COOH$, $R-COO^-$, and $R-COO^-Na^+$ have the units of mol/m^2), whereas the species that exist both in the bulk and at the surface (e.g., H^+ and Na^+) have the units of mol/m^3. Of course, c_{H^+} and c_{Na^+} refer to the concentrations of H^+ and Na^+ ions at the surface.

The total site density γ_C (having the units of 1/m^2) of –COOH groups can be expressed as [using eqs.(S3,S4)]:

$$\gamma_C = N_A\left[c_{R-COO^-} + c_{R-COOH} + c_{R-COO^-Na^+}\right] = N_A c_{R-COO^-}\left[1 + \frac{c_{H^+}}{K_a} + K_p\left(c_{Na^+}\right)\right] \tag{S5}$$

Therefore, we can express the pH-dependent charge density as:

$$\sigma_{ch,pH} = eN_A\left(c_{R-COO^-}\right) = \frac{e\gamma_C}{1+\frac{c_{H^+}}{K_a}+K_p\left(c_{Na^+}\right)} \qquad \text{(S6)}$$

In eqs. (S5,S6), N_A is Avogadro's number. Now the explicit relationship between $\sigma_{ch,pH}$ and the zeta potential (ζ) can be obtained by expressing c_{H^+} and c_{Na^+} (which are the concentrations at the surface) to their bulk or system values (i.e., $c_{H^+,\infty}$ and $c_{Na^+,\infty}$), by the Boltzmann distribution:

$$c_{H^+} = c_{H^+,\infty}\exp\left(-\frac{e\psi_{surface}}{k_BT}\right) = c_{H^+,\infty}\exp\left(-\frac{e\zeta}{k_BT}\right),\ c_{Na^+} = c_{Na^+,\infty}\exp\left(-\frac{e\psi_{surface}}{k_BT}\right) = c_{Na^+,\infty}\exp\left(-\frac{e\zeta}{k_BT}\right), \quad \text{(S7)}$$

where e is the electronic charge, k_BT is thermal energy, $\psi_{surface}$ is the electrostatic potential at the surface, i.e., the zeta potential (ζ).

Finally, using eq.(S7) in eq.(S6), we can write:

$$\sigma_{ch,pH} = eN_A\left(c_{R-COO^-}\right) = \frac{e\gamma_C}{1+\frac{c_{H^+,\infty}\exp\left(-\frac{e\zeta}{k_BT}\right)}{K_a}+K_pc_{Na^+,\infty}\exp\left(-\frac{e\zeta}{k_BT}\right)} \qquad \text{(S8)}$$

Consider $C_{H^+,\infty}$ and $C_{Na^+,\infty}$ are the concentrations expressed in M (mol/liter) [i.e., $c_{H^+,\infty} = 10^3C_{H^+,\infty} = 10^{3-pH_\infty}$ $\left(pH_\infty \text{ is the bulk pH}\right)$, $c_{Na^+,\infty} = 10^3C_{Na^+,\infty}$], so that eq.(S8) can be re-expressed as:

$$\sigma_{ch,pH} = \frac{e\gamma_C}{1+\frac{10^{3-pH_\infty}\exp\left(-\frac{e\zeta}{k_BT}\right)}{K_a}+K_p10^3C_{Na^+,\infty}\exp\left(-\frac{e\zeta}{k_BT}\right)}. \qquad \text{(S9)}$$

Eq.(S9) therefore provides the equation connecting the pH-dependent surface charge density to the zeta potential, bulk pH, and the salt concentration.

Of course, the zeta potential has been obtained experimentally at a given pH of 7 in Fig. 3(c) of

the main paper. Furthermore, we obtain zeta potentials experimentally as a function of the bulk pH as well as salt concentration. The results are provided in Fig. S4. Once the zeta potential is known experimentally, we can use eq.(S10) to obtain the pH-dependent charge density of the nanochannels.

Eq.(S9) can be simplified by noting that K_p is often very small [1] and using $\sigma_{ch} = e\gamma_C$, so that

$$\sigma_{ch,pH} = \sigma_{ch}\frac{K_a}{K_a + 10^{3-pH_\infty}\exp\left(-\frac{e\zeta}{k_BT}\right)} = \sigma_{ch}\frac{K_a}{K_a + \left(c_{H^+}\right)_{y=\pm h}} = \sigma_{ch}\frac{10^{-3}K_a}{10^3 K_a + \left(C_{H^+}\right)_{y=\pm h}}. \quad \text{(S10)}$$

In order to obtain the conductivity within the nanochannels, which in turn expresses the perm-selectivity of the nanochannels, we obtain the explicit potential and ion distributions in the electric double layer (EDL) near the charged nanochannel wall of the BC, as described by Gouy-Chapman Poisson-Boltzmann equation:

$$\frac{d^2\psi}{dy^2} = -\frac{\sum_i z_i e n_i}{\varepsilon_0 \varepsilon_r}. \quad \text{(S11)}$$

$$n_i = n_{i,\infty}\exp\left(-\frac{z_i e\psi}{k_BT}\right) \quad \text{(S12)}$$

In eqs. (S11, S12), n_i, $n_{i,\infty}$, and z_i are the local ion number density, bulk ion number density and valence of the ionic species i (i = ±; H^+;OH^-). We assume that we add an acid that furnishes the same anion as the electrolyte salt; consequently, $n_{+,\infty} = n_\infty$ and $n_{-,\infty} = n_\infty + n_{H^+,\infty}$. Eq. (S11) will obviously be simplified by using eq. (S12) to replace the ion number densities in terms of ψ. This resulting equation in ψ will be solved in the presence of the following boundary conditions:

$$\left(\frac{d\psi}{dy}\right)_{y=\pm h} = -\frac{\sigma_{ch,pH}}{\varepsilon_0 \varepsilon_r}, \quad \left(\frac{d\psi}{dy}\right)_{y=0} = 0. \tag{S13}$$

Eqs. (S10), along with the knowledge of the experimental zeta potential (see Fig. 3c) are used to express $\sigma_{ch,pH}$ for both the pristine BC and TEMPO BC.

The conductivity is measured by applying an axial electric field *E*, which triggers an ionic current *I*:

$$I = eE \int_{-h}^{h} \left(\sum_i \mu_i n_i \right) dy \tag{S14}$$

In eq. (S14), μ_i is the electrophoretic mobility of ionic species *i.* Using eq. (S12) to express n_i and using the appropriate expressions for $n_{i,\infty}$, we can finally obtain the ionic conductivity (σ) from eq. (S14) as:

$$\begin{aligned} \sigma &= \frac{I}{2hE} = e \int_{-1}^{0} \left(\sum_i \mu_i n_i \right) dy \\ &= e n_\infty \int_{-1}^{0} [\mu_+ \exp(-\bar{\psi}) + \mu_- (1 + \bar{n}_{H^+,\infty}) \exp(\bar{\psi}) \\ &+ \mu_{H^+} \bar{n}_{H^+,\infty} \exp(-\bar{\psi}) + \mu_{OH^-} \bar{n}_{OH^-,\infty} \exp(\bar{\psi})] d\bar{y}. \end{aligned} \tag{S15}$$

In eq. (S15), $\bar{y} = \frac{y}{h}$, $\bar{\psi} = \frac{e\psi}{k_B T}$, $\bar{n}_{H^+,\infty} = \frac{n_{H^+,\infty}}{n_\infty}$, and $\bar{n}_{OH^-,\infty} = \frac{n_{OH^-,\infty}}{n_\infty}$.

Note that the charged surface always requires a certain amount of couterions inside the channel to neutralize the system. Therefore at low concentration, surface charge density dominates the conductivity and eq. (S15) can be simplified as:

$$\sigma \sim \frac{\mu_+ \sigma_{ch,pH}}{h}. \tag{S16}$$

Therefore it is witnessed that conductivity is almost a constant number (at a given bulk pH) at

low concentration (see Fig. 3b). Note that the ionization can be affected if the ionization constant K_a is small: a decrease in pH or salt concentration may dramatically decrease the surface charge density. On the contrary, the surface charge density is less affected with a larger K_a; it is witnessed that at $C_\infty = 10^{-6}$ M, the conductivity is slightly higher. That is because at such low salt concentration, the number density of hydrogen ions n_{H^+} becomes comparable to the number density of sodium ions n_+ inside the channel, and hence plays a role in neutralizing the charged surface. The mobility of H^+ ions is much larger, resulting in a higher conductivity at such low concentration given the fact that pH = 7 (see Fig. 3b).

At a large salt concentration, the EDL is very negligible compared to the channel size and accordingly the screening of the EDL double layer occurs at the immediate vicinity of the charged nanochannel – as a consequence, the bulk solution dominates the conductivity:

$$\sigma \sim e n_\infty \left(\mu_+ + \mu_-\right). \qquad \text{(S17)}$$

Therefore, in the log-log variation of the conductivity versus concentration c_∞ (where $n_\infty = 10^3 N_A c_\infty$) the plot is a straight line with a 45 degree slope with respect to the x-axis. This also explains the origin of variations in conductivity for pristine BC and TEMPO BC at larger salt concentrations.

Finally, by treating the conductive material as a porous medium, the effective conductivity (σ_p) becomes:

$$\sigma_p \sim \sigma f, \qquad \text{(S18)}$$

where f is the medium porosity. In Fig. 3(b), we plot σ_p (where σ is obtained using eq. S7) for the different types of BC. Furthermore, to obtain these predictive plots, we use, for pristine BC, $f = 0.15, \sigma_{ch} = -0.4\, mC/m^2,\ 2h = 2\, nm,$ while for the TEMPO-treated BC, $f = 0.2, \sigma_{ch}$

$= -6\,mC/m^2$, $2h = 1\,nm$. Other parameters are $\mu_+ = \mu_{Na^+} = 5.19 \times 10^{-8}\,m^2/Vs$, $\mu_- = \mu_{Cl^-} = 7.9 \times 10^{-8}\,m^2/Vs$, $\mu_{H^+} = 36 \times 10^{-8}\ m^2/Vs$, $\mu_{OH^-} = 20 \times 10^{-8}\,m^2/Vs$, $\varepsilon_0 = 8.8 \times 10^{-12}\,C/(Vm)$, $\varepsilon_r = 79.8$, $k_B = 1.38 \times 10^{-23}\,J/K$, $T = 300$ K, and $e = 1.6 \times 10^{-19}\,C$. With these parameter values (i.e., values of the surface charge densities and pore diameters), our theory provides an excellent match for the experimental results of the NaCl-concentration-dependent conductivity of the pristine BC and TEMPO-treated BC. The smaller channel size fit for TEMPO-treated BC than pristine BC can be justified due to the increased hydrophilicity after TEMPO treatment, which can cause additional swelling of the cellulose nanofibers. Additional swelling of the film within the confined space will result in a smaller channel size.

In the end, it is useful to re-iterate that we have conducted experiments to show how the zeta potential varies with pH and salt concentration (see Fig. S4). There is insignificant variation in the zeta potential with salt concentration, but large variation with pH. The variation in zeta potential with pH follows the dependence of $\sigma_{ch,pH}$ on pH as given explicitly by eq.(S9,S10). Given that the perm-selectivity (dictated by the electrical conductivity) is governed by the electrostatic potential distribution, which in turn is dictated by the pH-dependent surface charge density ($\sigma_{ch,pH}$) at the nanochannel walls, one can associate a strong pH dependence with the perm-selectivity

Consideration of other electrokinetic effects

The entire theoretical derivation in the previous section has essentially ignored any ion distribution in the axial direction, i.e., along the length of the nanochannel (or the direction of propagation of ionic current). On the other hand, more rigorous analysis derived from explicit knowledge of the detailed BC structure, would include several other factors that can alter the electrokinetics of the system. While consideration of these effects is beyond the scope of the present study, we do identify them here for future consideration in the context of ionic transport in BC.

Donnan Equilibrium

Donnan equilibrium refers to the equilibrium distribution of a given type of ion across a semi-permeable or fully permeable membrane (i.e., across a finite axial distance across the membrane)[3,4]. The same formulation has been conveniently applied to understand the development of axial ion equilibrium at the interface between a microchannel and a nanochannel, with this interface being treated as an equivalent *membrane*[5]. The development of this axial ion distribution at the nanochannel-inlet-microchannel interface as well as the nanochannel-outlet-microchannel interface will lead to the development of an electrostatic potential gradient along the axial direction, which has been calculated in detail previously[5]. In the present study, we are quantifying the conductivity of the nanochannels by employing an axial electric field and measuring the resulting current. Of course, in our calculation we assumed the presence of no such pre-existing axial potential gradient. Therefore, we obtained the conductivity by taking the ratio of the developed current and the applied electric field. On the other hand, recent studies have shown that the overall potential difference and the resulting electric current in a

microchannel-nanochannel system will be dictated by the interplay of this induced axial potential gradient (associated with the Donnan equilibrium) and the imposed axial electric field[6] [R7]. Therefore, more detailed analysis, which is beyond the scope of the present study, would necessitate the consideration of this particular situation. While we endeavor to take up such an analysis in a future study, we apprehend that the key bottleneck of such an analysis would be a precise definition of the complicated network of the micro-nanochannels that characterize the BC architecture.

Concentration Polarization

Very much like the Donnan equilibrium, concentration polarization (CP) is also a phenomenon that characterizes the behavior at the junction of a micro-nanochannel[7,8]. Very often the pronounced effect of an electric double layer in a nanochannel would imply that the counterion (coion) concentration is much higher (lower) inside the nanochannel as compared to that within the microchannel. Under such a situation, if an electric field is applied, there will be axially separated zones where both the counterions and coions are simultaneously enriched or depleted[7–9]. This is known as CP, which has been widely investigated under different situations. In few recent papers, Santiago and co-workers reported that this CP could be either non-propagating or propagating (as a shock wave)[8,10]. Such propagation is likely if (for a monovalent and symmetric salt)

$$-\frac{\left(\mu_{+}+\mu_{-}\right)Fhc_{\infty}}{2\mu_{+}\sigma_{ch,pH}} < \max\left(\mu_{-}^{*}, 2\mu_{-}^{*}-1\right) \left[\text{where } \mu_{-}^{*}=\frac{\mu_{-}F\eta}{\varepsilon_{0}\varepsilon_{r}\zeta}\right], \tag{S18}$$

where F is the Faraday's constant and η is the dynamic viscosity of water. For our case, we obtain

$$\left(-\frac{(\mu_+ + \mu_-)Fhc_\infty}{2\mu_+\sigma_{ch,pH}}\right)_{C_\infty=1M} = 17.5,\ \left(-\frac{(\mu_+ + \mu_-)Fhc_\infty}{2\mu_+\sigma_{ch,pH}}\right)_{C_\infty=10^{-6}M} = 17.5\times10^{-6},\ \text{and}\ \mu_-^* = 2.8\times10^4 \qquad \text{(S19)}$$

Combining eqs.(S18,S19), we can witness propagation of CP shocks in the nanochannel system. Of course, here too, we would need a detailed understanding of the microchannel-nanochannel architecture of the BC to account for the effect of the CP and the possible CP shocks traversing the BC system. Therefore, this analysis is also beyond the scope of the present study.

References

(1) Das, S.; Subramanian, K.; Chakraborty, S. Analytical Investigations on the Effects of Substrate Kinetics on Macromolecular Transport and Hybridization through Microfluidic Channels. *Colloids Surfaces B Biointerfaces* **2007**, *58*, 203–217.

(2) Das, S.; Thundat, T.; Mitra, S. K. Analytical Model for Zeta Potential of Asphaltene. *Fuel* **2013**, *108*, 543–549.

(3) CHAUDHURY, S. G. The Donnan Membrane Equilibrium. *Nature* **1943**, *152*, 76.

(4) Philipse, A.; Vrij, A. The Donnan Equilibrium: I. on the Thermodynamic Foundation of the Donnan Equation of State. *J. Phys. Condens. Matter* **2011**, *23*.

(5) Tian, H.; Zhang, L.; Wang, M. Applicability of Donnan Equilibrium Theory at Nanochannel-Reservoir Interfaces. *J. Colloid Interface Sci.* **2015**, *452*, 78–88.

(6) Guan, W.; Reed, M. A. Electric Field Modulation of the Membrane Potential in Solid-State Ion Channels. *Nano Lett.* **2012**, *12*, 6441–6447.

(7) Baldessari, F. Electrokinetics in Nanochannels. Part I. Electric Double Layer Overlap and Channel-to-Well Equilibrium. *J. Colloid Interface Sci.* **2008**, *325*, 526–538.

(8) Zangle, T. A.; Mani, A.; Santiago, J. G. Theory and Experiments of Concentration Polarization and Ion Focusing at Microchannel and Nanochannel Interfaces. *Chemical Society Reviews*. 2010, pp 1014–1035.

(9) Das, S.; Dubsky, P.; Van Den Berg, A.; Eijkel, J. C. T. Concentration Polarization in Translocation of Dna through Nanopores and Nanochannels. *Phys. Rev. Lett.* **2012**, *108*.

(10) Zangle, T. a; Mani, A.; Santiago, J. G. On the Propagation of Concentration Polarization from Microchannel−Nanochannel Interfaces Part II: Numerical and Experimental Study. *Langmuir* **2009**, *25*, 3909–3916.